ACS APPLIED MATERIALS & INTERFACES

Research Article

www.acsami.org

Wet Adhesion of Buckypaper Produced from Oxidized Multiwalled Carbon Nanotubes on Soft Animal Tissue

Andrea Martinelli,[†,*] Giovanna A. Carru,[‡] Lucio D'Ilario,[†] Fabrizio Caprioli,[†] Massimo Chiaretti,[‡] Fernanda Crisante,[†] Iolanda Francolini,[†] and Antonella Piozzi[†]

[†]Department of Chemistry, Sapienza University of Rome, P.le Aldo Moro 5, 00185 Rome, Italy

[‡]Department of General Surgery "Paride Stefanini", Sapienza University of Rome, Viale del Policlinico 155, Rome 00161, Italy

Supporting Information

ABSTRACT: Buckypaper (BP) is the general definition of a macroscopic assembly of entangled carbon nanotubes. In this paper, a new property of a BP film produced from oxidized multiwalled carbon nanotubes was investigated. In particular, BP shows to be able to promptly and strongly adhere to animal internal soft and wet tissues, as evaluated by peeling and shear tests. BP adhesion strength is higher than that recorded for a commercial prosthetic fabric (sealed to the tissue by fibrin glue) and comparable with that of other reported optimized nanopatterned surfaces. In order to give an interpretation of the observed behavior, the BP composition, morphology, porosity, water wettability, and mechanical properties were analyzed by AFM, X-ray photoelectron spectroscopy, wicking tests, contact angle, and stress−strain measurements. Although further investigations are needed to assess the biocompatibility and safety of the BP film used in this work, the obtained results pave the way for a possible future use of buckypaper as adhesive tape in abdominal prosthetic surgery. This would allow the substitution of conventional sealants or the reduction in the use of perforating fixation.

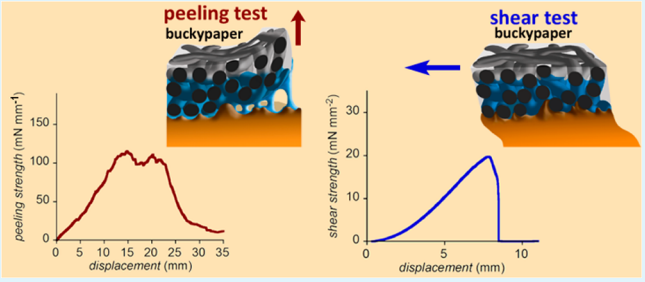

KEYWORDS: *buckypaper, multiwalled carbon nanotube, adhesion, animal tissue, prosthesis*

INTRODUCTION

In the last years, extensive research has been focused on the adhesive pads of climbing animals, like lizards, spiders, insects, and frogs.[1] Their ability to reversibly adhere on smooth or rough and dry or wet surfaces can, indeed, inspire new functional materials. Mimiking the animal strategy, structured surfaces endowed either with nano or micropillars (setae) or with micro or nanochannels were prepared and tested for their ability to adhere on smooth or rough substrates.[2] It was observed that for a strong but reversible adhesion on a rigid substrate, a hierarchical (fractal-like) nanostructured construction is necessary. Indeed, this construction is able to reduce the elastic deformation energy between the patterned and the rough surface to decrease the pull-off force during locomotion and to avoid setae buckling and bundling.[3] Moreover, to prevent rapid material deterioration and contamination as well as to allow rapid attachment and detachment cycles, the adhesive surfaces should be made of stiff materials.

So far, only few studies have focused on the design of materials able to permantly adhere on smooth compliant surfaces in wet condition.[4,5] These materials could find important application in the biomedical field. In fact, the availability of adhesive materials for biological surfaces could solve many medical and surgical problems found when artificial systems must strongly adhere on wet mammalian tissues under physiological conditions.

The effect of properties of rigid surfaces on their adhesion to soft compliant substrates was studied and modeled by Persson who described the capillary adhesion of an elastic soft solid onto a rough hard surface.[6] He pointed out the importance of (i) the increase in the contact area between the soft and the hard substrate due to the deformation of the soft solid that, driven by the capillary adhesive force, comforms to the surface of the hard substrate and (ii) the negligible repulsive interfacial elastic forces, as a result of the low modulus of almost one material. In addition, the presence of nano-asperities and nanopores on the rigid surface can promote the formation of a network of nanocapillary bridges during the pull-off and facilitate the squeeze-out of fluid excess between the two surfaces.[7] Prompted by these suggestions, with the intent to find a material able to permanently adhere on animal wet tissues, we focused our attention on a relatively new material, the buckypaper (BP) that is a macroscopic self-supporting film composed of entangled carbon nanotubes (CNT).[8] Actually, BP is a general definition of a class of materials displaying

Received: February 8, 2013
Accepted: April 18, 2013
Published: April 18, 2013

different properties according to its composition or preparation conditions and methods. Single, double, multiwalled CNTs with different lengths, diameters, or aspect ratios can be used to prepare BP. Besides the intrinsic properties of the components, BP can show additional interesting features exploitable in various technological fields for the fabrication of composites, field emission sources, or electronic devices. Moreover, boosted by the intense research on CNT application in the biomedical fields,[9] some studies were recently focused on the use of BP for the preparation of medical devices. Particularly, BP has been proposed for the encapsulation of islet cells for diabete treatment, as an artificial membrane for retinal and iris pigment epithelial transplantation, as a flexible antiseptic bandage, as immune shielding for cells and tissues, as a carrier for gene or drug delivery, and as a scaffold for tissue engineering.[10−15] Moreover, BP has suitable conductivity and mechanical properties to be used for the manufacturing of implantable electrodes for nerve sensing and stimulation, pacemaker electrodes, and electrocardiogram pads.[16−18] As far as the biocompatibility is concerned, BP was recently shown to be not toxic and to not affect the in vitro proliferation and viability of both normal human arterial smooth muscle cells and human dermal fibroblasts.[19] Moreover, multiwalled carbone nanotube (MWCNT)-based 3D networks were able to support the attachment and growth of mouse fibroblasts.[15] In vivo experiments, carried out on rats showed that although the BP used in this work induced a moderate inflammatory reaction, it had no mutagenic effects. A cicatrization reaction with a scar organization and fibrosis was recorded two weeks after BP implantation.[19]

In the present paper, we studied the adhesive properties of BP on a wet compliant substrate. In particular, a flexible 0.15−0.25 mm thick film of unoriented oxidized multiwalled carbon nanotubes was used. The material selection was done according to the right combination of porosity, roughness, mechanical properties, and hydrophilicity to accomplish the task. Shear and peeling adhesion tests showed that BP readly and strongly adhered to a trimmed muscular fascia of a rabbit abdominal wall, chosen as the model substrate. The results of BP adhesion strength were compared to those obtained by using a commercial polytetrafluoroethylene prosthetic fabric either simply placed onto the tissue or fixed to the tissue by human fibrin glue. Moreover, a detailed characterization of BP chemical and physical properties, which are retained crucially in the definition of BP adhesive behavior, was carried out. As a tissue adhesive material, BP could find application in abdominal prosthetic surgery or for wound closure, thus allowing not only easier surgery procedures but also reduction in the use of conventional perforating fixation, to which serious post-operative complications are usually associated.

EXPERIMENTAL SECTION

Material. Commercial buckypaper (BP) from Nanolab, Inc. was used in this study because its biocompatibility was already tested by our group both in vitro and in vivo.[19] They used BP is a microporous nanoporous flexible felt, about 0.15−0.25 mm thick, composed of entangled unoriented MWCNT. According to the supplier information, hydrochloric and nitric acid-treated MWCNT were first suspended in water with a surfactant and then filtered on a membrane. A free-standing continuous nanotube sheet was obtained. Because of the BP preparation and drying process used by the producer, the resulting nanotube sheet was characterized by a surface asymmetry. In particular, one side was glossy, compact, and smooth (hereafter defined as BP_s), while the other side was highly porous and rough (hereafter defined as BP_r). This asymmetry allowed evaluating the influence of surface morphology on BP adhesion properties. In order to remove catalysts and surfactant residues, the supplied BP was rinsed with 6 N nitric acid water solution and deionized water and then vacuum dried at 90 °C.

AFM Analysis. The BP surface morphology was investigated by a Bruker Multimode atomic force microscope (AFM) with a NanoScope 3d digital controller. The analysis was carried out in tapping mode, at room temperature, and under ambient conditions by using a RTEPS probe with a nominal curvature radius of 8 nm.

XPS Analysis. X-ray photoelectron spectroscopy (XPS) measurements were performed by using a modified Omicron MXPS system with a dual anode X-ray source (Omicron DAR 400), an Omicron EA-125 energy analyzer, and a nonmonochromatized Mg Kα photon ($h\nu$ = 1253.6 eV) generator operating the anode at 14 kV and 16 mA. All the reported XP spectra were acquired using an analyzer pass energy of 20 eV and a takeoff angle of 11° with respect to the surface normal. The measurements were carried out at room temperature with an initial pressure in the analyzer chamber lower than 2×10^{-9} mbar. No evidence of sample degradation or charging effects under the X-rays, such as band broadening or progressive shift, were observed during the experiments. The binding energy (BE) of the main C1s line (attributable to sp^2 graphite carbon) at 284.1 eV was used as internal standard reference. The experimental spectra were theoretically reconstructed by fitting with symmetric Voigt functions letting the Gaussian−Lorentzian ratio free to vary between 50% and 100%. The quantitative analysis was performed correcting the peak areas with the corresponding Scofield cross sections.

Stress−Strain Tensile Experiments. Tensile mechanical properties were measured by an Instron 4502 Universal Testing Machine with a 2 kN load cell at a cross-head speed of 10 mm min^{-1} on 10 mm × 2.5 mm × (0.150−0.250) mm sample strips cut with a scalpel from dry or wet BP. Wet BP was obtained by dwelling it in deionized water for 1 h. Stress−strain curves were reported as the apparent stress $\sigma = F/A$ (MPa), where F is the tensile force and A is the initial cross-sectional area of each test specimen, versus the strain $\varepsilon = (L - L_0)/L_0$, where L_0 and L are the initial and the deformed sample lengths, respectively. The Young modulus was calculated as the slope of the steepest region of the stress−strain curve.

Wicking Test. The BP used in this study is a highly hydrophilic material that absorbs water rapidly. This behavior depends on the MWCNT chemical surface composition and morphological features. As shown by XPS analysis, the partial oxidation carried out by nitric acid treatment introduced oxidized carbon atoms mainly on the edges or defects of the MWCT. Moreover, as fibrous nonwoven fabric, BP has a heterogeneous structure consisting of entangled nanotubes or nanotube bundles. The internanotube network is composed of unoriented capillary channels with a heterogeneous distribution of dimensions. The characterization at microscopic level of such complex morphology could be quite difficult. Alternatively, the BP pore network dimension can be estimated by the vertical wicking test that gives information on the mean equivalent radius of the cylindrical capillary approximating the internanotube channels. The capillary liquid adsorption (wicking) was evaluated by suspending a 10 × 30 mm^2 BP strip to the hook of the Wilhelmy balance (Cahn 312). The liquid was moved up until it contacted the BP bottom surface. Then, the mass variation of the sample was automatically recorded as a function of time.

The capillary rise of a liquid into a wettable porous solid can be described by the Lucas−Washburn equation

$$\frac{dL(t)}{dt} = \frac{R^2}{8\eta L(t)}\left(\frac{2\gamma \cos \vartheta}{R} - \rho g L(t)\right) \quad (1)$$

where $L(t)$ is the height of the liquid front at time t, R is the mean equivalent pore radius, η is the liquid viscosity, γ is the surface tension of the liquid, and ϑ is the contact angle that the liquid forms with the pore wall.[21] The second term in brackets takes into account the hydrostatic pressure P_h, where ρ is the liquid density, and g is the

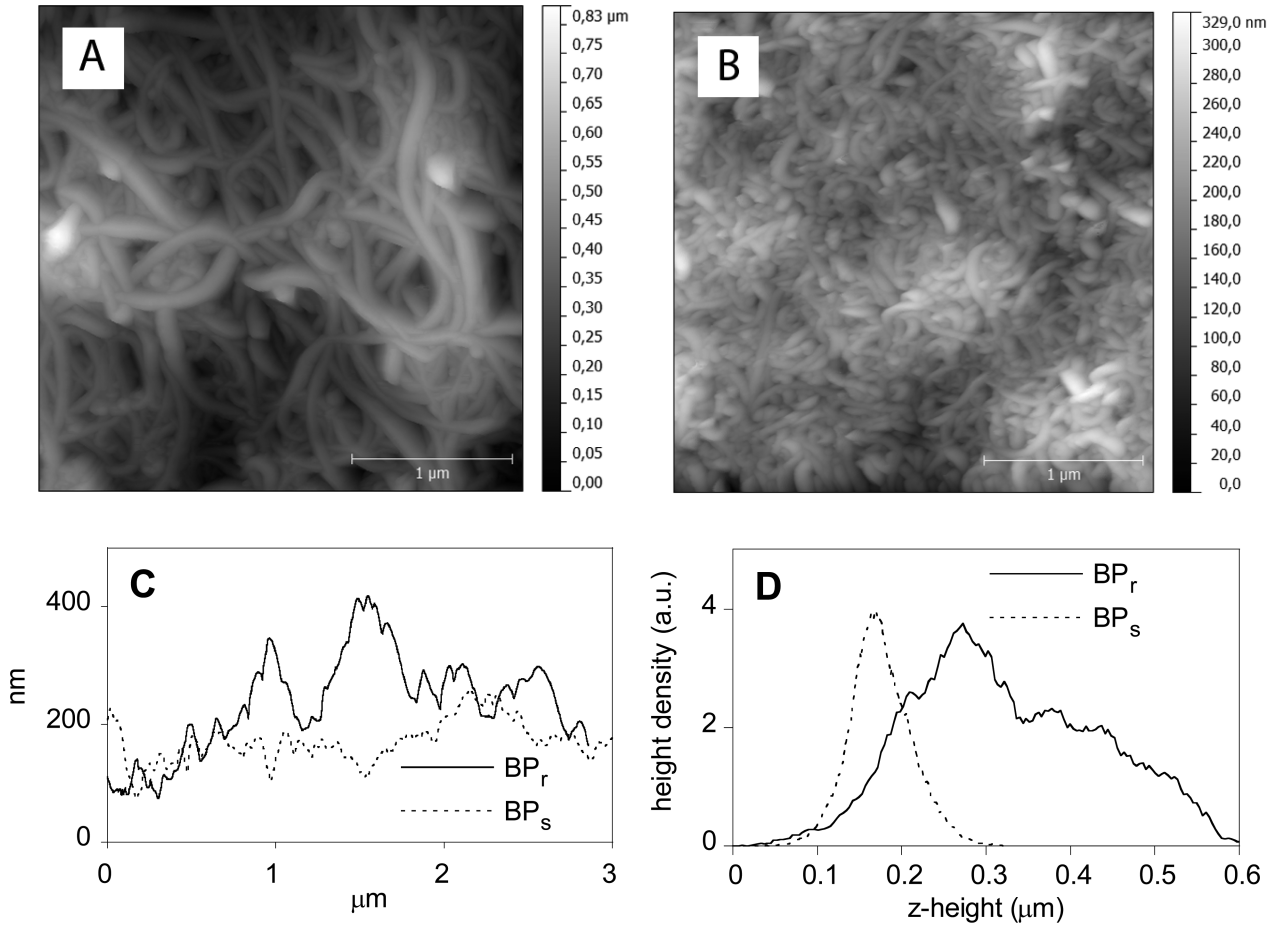

Figure 1. AFM analysis. AFM height images of BP_r (A) and BP_s (B). Comparison of the height profile (C) and *z*-height distribution (D) of BP_r and BP_s.

gravity acceleration constant. In the early stage of the wicking process, $P_h \sim 0$, and eq 1 can be simplified in

$$L(t)^2 = \frac{R\gamma \cos \vartheta}{2\eta} \times t \tag{2}$$

The wicking test is usually carried out by recording the liquid front height as a function of time. Because the buckypaper is black, it was not possible to observe the level $L(t)$ during the liquid rise. Therefore, the liquid uptake mass $m(t)$ as a function of the wicking time was measured, being $m(t)$ is related to $L(t)$ by the following equation

$$L(t)_{calc} = \frac{m(t)}{A\varepsilon\rho} \tag{3}$$

where A is the geometric area of the BP sample bottom surface, ε is the BP porosit, and ρ is the liquid density. The porosity ε is defined as

$$\varepsilon = \frac{V_v}{V_{BP}} = \frac{1 - V_{MWCNT}}{V_{BP}} \tag{4}$$

where V_v is the volume of the internanotube voids, V_{BP} is the geometric volume of the BP sample, and V_{MWCNT} is the volume of the carbon nanotubes. ε was evaluated by a hydrostatic balance, weighting the BP sample before and after immersion either in water or *n*-dodecane. The experiments carried out with the two liquids gave a porosity value of $\varepsilon = 0.79 \pm 0.1$. Therefore, an apparent BP density of $\rho_{BP} = 0.30 \pm 0.03$ g cm^{-3} and a MWCNT density of $\rho_{MWCNT} = 1.7 \pm 0.2$ g cm^{-1} can be inferred. This latter value is in good agreement with the data reported in the literature.[22,23] As for the contact angle that the liquid forms with the BP_r and BP_s surface because of the rapid liquid diffusion in the porous material, it was not possible to directly measure it by static goniometric or dynamic tensiometric techniques. In order to decrease the liquid infiltration rate, the porosity was reduced by pressing BP at 40 MPa between two smooth stainless steel plates. By deposition of a water drop (about 5 μL) on each BP surface and by using an image acquisition system, a stable water static contact angle of $\vartheta = 83° \pm 2°$ was measured on both surface sides of the compressed BP foil. Because this measurement is influenced by the surface BP roughness and heterogeneity, the found value does not represent the contact angle that the single nanotube form with water. However, it is in good agreement with the values found by Barber et al.[24] on single nitric acid-treated MWCNT and by Mattia et al. on 60−300 nm chemical vapor deposition (CVD)-carbon nanopipes.[25]

As for the *n*-dodecane, this solvent rapidly diffused also into the compressed BP foil because of its low surface tension. Therefore, a $\vartheta = 0°$ was used in eq 2.

Adhesion Tests. The adhesion strength of BP rough and smooth surfaces to the biological tissue was evaluated by peeling and shear tests by using wet animal internal tissue. The measurements were carried out by an Instron 4502 universal testing machine at a crosshead speed of 10 mm min^{-1} and a 10 N measuring cell. A 3.5cm × 2.5 cm sample about 0.5−1 cm thick of trimmed muscular fascia of the abdominal wall of New Zeeland female rabbits was fixed on a Plexiglas plate by means of a four spring-driven frame endowed with a 2.5 cm × 2.5 cm central window.

In the peeling tests, about 3−4 mm portion of a 2 cm × 2 cm square-shaped dry BP sample was clamped to the grip and connected to the upper mobile measuring cell of the testing machine by a freely tilting 18 cm stainless steel wire. In this way, the nominal peel angle variation during the test can be considered negligible (±6°). Either the smooth or rough BP surface was then placed manually onto the horizontally mounted wet biological substrate and pulled at a 90° angle within 30 s.

The shear tests were instead performed to assess the BP adhesion strength to the tissue when stressed by lateral movement. In particular, a 0.5 cm × 2 cm portion of dry BP was laid on the vertically mounted biological substrate and pulled in the direction parallel to the sample−substrate interface. Both the peeling and shear tests were recorded 30 s after BP deposition onto the biological substrate. Longer time periods had no influence on the adhesion strength.

After detachment, the sample surface was visually observed. The clean peeling of the BP from the substrate was indicative of adhesive failure, whereas the fracture or the presence of residues of the biological tissue on the BP surface was indicative of cohesive failure.

Peeling and shear tests were also carried out on the commercial porous prosthetic membrane Dulex Bard (DB, Bard), a soft polytetrafluoroethylene fabric characterized by a microporous structure on one side (able to minimize visceral attachment) and a macroporous structure on the other side designed to promote tissue in-growth. Sample dimensions and test procedures were similar to those used to characterize BP. The Dulex Bard macroporous side was either simply placed onto the biological tissue or fixed to the tissue by human fibrin glue (Tissucol, Baxter Healthcare). In this latter case, a thin layer of glue was first deposited on the tissue, and then the Dulex Bard membrane was laid down and let to adhere for 5 min before performing the tests.

The animals used in the experiments were treated in accordance with the policies and principles of standard laboratory animal care and with the European Union guidelines (86/609/EEC) approved by the Italian Ministry of Health and by General Surgery Department Council (authorization n°159/20010-20 September, 2010).

RESULTS AND DISCUSSION

AFM Analysis Results. The AFM images of the rough and smooth BP side (BP_r and BP_s, respectively) as well as their *z*-height distribution and representative height profile are displayed in Figure 1.

The mean CNT diameter, root mean squared (rms) roughness, and surface roughness (SR), defined as the ratio between the surface area (computed by simple triangulation) and the projected surface area (3 μm × 3 μm), were evaluated from AFM height images by Gwyddion software (Table 1).

Table 1. AFM Height Image Analysis Results[a]

sample	mean CNT diameter (nm)	rms roughness (nm)	SR[b]
BP_r	90 ± 30	110 ± 5	1.9
BP_s	60 ± 20	50 ± 20	1.3

[a]Each data represents the mean value of scans on almost three different 3 μm × 3 μm sample portions. [b]Ratio between the surface area (computed by simple triangulation) and the projected surface area.

AFM analysis enlightened a great morphology difference between the two BP sides. The BP_r surface showed large MWCNT or MWCNT bundles, aggregated in a highly porous structure (Figure 1A). The *z*-height distribution (Figure 1D), rms roughness, and SR values evidenced a nubby morphology, characterized by about 200−300 nm deep and 500 nm large wells (Figure 1C). On the contrary, the BP_s side showed a smoother and more compact aggregation of CNT having a smaller mean diameter (Table 1). Moreover, both the height profile (Figure 1C) and *z*-height distribution (Figure 1D) revealed a flatter surface of BP_s than BP_r . Because the supplier documentation reports that BP is composed of MWCNT with an outer diameter of 15 nm, we supposed that the found larger diameter of nanotubes is due to the presence of close-packed MWCNT bundles as a result of van der Waals interactions.[26] These aggregates were stable because no morphology variation was observed between water dwelled and dried BP samples.

XPS Analysis Results. XPS analysis was carried out to assess the surface composition and oxidation degree of BP MWCNT. The BP was produced from preoxidized MWCNT, and XPS analysis did not evidence significant compositional differences between the two faces that differ just in the morphology. In Figure 2, the XPS spectrum of the rough BP surface is reported. When found, the small composition variations between BP_s and BP_r are reported.

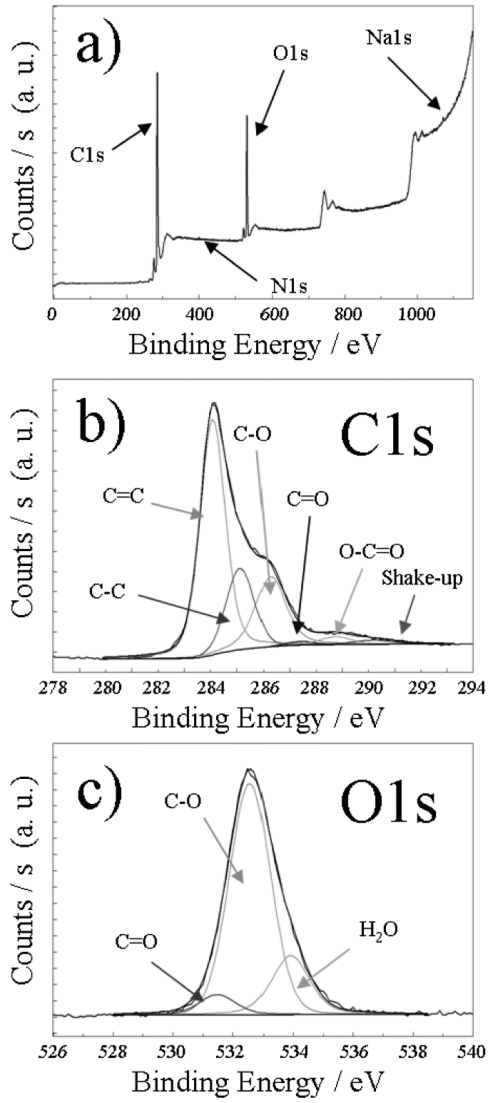

Figure 2. XPS spectra of BP. (a) Survey scan spectrum. (b) C1s XP spectrum. (c) O1s XP spectrum.

The two main peaks lying at ∼285 eV and ∼530 eV in the survey scan spectrum of buckypaper (Figure 2A) were attributed to the C1s and O1s core lines, respectively.

The quantitative analysis revealed an O/C atomic ratio of 0.23 (0.25 for BP_s) that indicates a high level of nanotube oxidation if compared to the data reported in the literature for similar systems.[27−31] The small signals at ∼1072 eV and ∼400 eV can be attributed to traces (less than 1%) of sodium and nitrogen, respectively, presumptively arising from either the MWCNT synthesis and oxidation processes or BP preparation. The deconvolution of C1s and O1s peaks, reported in Figure

2B and C, respectively, allows identifying and quantifying the various oxidation products. The best fit of the asymmetric C1s spectrum revealed the presence of six components, indicating that the treatment with HNO_3 led, as expected, to a complex composition.[27−31] In accordance with several literature reports, the main peak in the C1s region, lying at the lower binding energy, was attributed to sp^2 graphitic carbon.[27−30] The signal at 285.1 ± 0.2 eV was assigned to sp^3 carbon, likely related to the formation of some defects in the MWCNT due to the partial destruction of the π-conjugated system during the oxidation process .[27,28] However, the attribution of this signal is still in debate in the literature. In fact, it has been also associated to the presence of some unsaturated sp^2 carbon atoms (dangling bonds) or to the formation of amorphous structures.[27,32] The three components centered at 286.2 ± 0.2, 287.4 ± 0.2, and 288.7 ± 0.2 eV can be assigned to different oxidized carbons and, in particular, to carbons involved in a single bond with one oxygen atom (phenols and ethers), to carbons having a double bond with one oxygen atom (ketones, aldheyds, and quinones), and to carboxylic groups (carboxylic acid and esters).[27−31] The ratios between these components showed that phenols and/or ethers are the main oxidation products on the MWCNT, followed by carboxylic groups.

A very small amount of carbonyl carbons (~20 times less than C−O carbons) was also detected, suggesting that these species are quickly further oxidized to carboxyl during the treatment with HNO_3. Finally, the broad peak centered at 290.2 ± 0.2 eV was ascribed to the typical shake up line of aromatic carbon compounds due to a $\pi \rightarrow \pi^*$ transition.[27−30] The analysis of the O1s region essentially confirmed the results discussed above. The deconvolution of the O1s peak resulted in three signals at 531.5 ± 0.2, 532.6 ± 0.2, and 533.9 ± 0.2 eV. The first two peaks can be respectively assigned to C−O (phenols, ethers, and single-bonded oxygen in carboxylic groups) and C═O oxygen (ketones, aldheyds, quinones, and double-bonded oxygen in carboxylic groups) present on the surface of MWCNT.[29,31] The component at a higher binding energy was assigned to residual water molecules. The high ratio found between the C−O peak and C═O signal (about 10:1) confirmed the preponderance of phenols and ethers group with respect to other oxidation products. Moreover, because the carboxylic groups contributed to both C−O and C═O components, this quantitative analysis is in good agreement with the fit performed on C1s spectrum.

Wicking Test Results. When immersed in water or *n*-dodecane, BP rapidly adsorbed the liquid, without any change in dimension, as verified by optical microscopy observations. The total water uptake after BP dwelling in water for 1 h was evaluated to be about 4 times BP dry weight, as expected from its porosity. Despite the nanometric size, the MWCNT rigidity, both in tensile and bending mode, prevented large nanotube rearrangements.[33] Different than from other softer nonwoven hydrophilic fabrics such as cellulose paper,[34] sample contraction at low water content due to interfiber capillary attractive forces or swelling at high water content was negligible and, hence, eq 3 can be safely used. The values of the test liquid properties present in eqs 2 and 3 are reported in Table 2.

The typical $L(t)_{calc}$ variation, calculated from the BP weight uptake according to eq 3, as a function of wicking time in water and *n*-dodecane, is reported in Figure 3.

The curves were interpolated by eq 2 and the *R* values for the two liquids, calculated from the curve fitting, are reported in Table 2. Data are the mean of five measurements (±SD). With both liquids, a mean equivalent pore radius in the order of magnitude of 10 nm was obtained.

Table 2. Physical Properties of Liquids Employed in Eqs 2 and 3 and Mean Value of BP Equivalent Pore Radius *R*

liquid	η (Pa s)	ρ (kg m^{-3})	γ (J m^{-2})	ϑ (deg)	*R* (nm)
Water	1.01×10^{-3}	1000	72.8×10^{-3}	83 ± 3	12 ± 4
n-Dodecane	1.34×10^{-3}	746	25.35×10^{-3}	0	7 ± 3

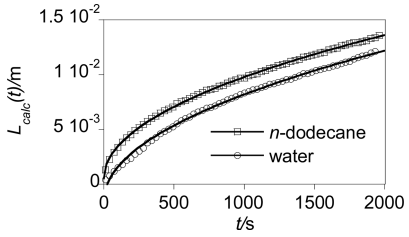

Figure 3. Liquid front height, calculated from BP weight uptake by eq 3, as a function of the wicking time. Solid lines are the best fit curves from eq 2.

It is worth noting that the *R* value represents the radius of equivalent capillaries driving the water wicking into the porous material and may differ from the actual dimension of the nonuniform and tortuous internanotube channels. In fact, the AFM image of Figure 1A showed that the presence of pores larger than 50 nm, even if offering a minor resistance to liquid flow, contribute a lesser extent to the negative capillary pressure.

Mechanical Properties. The stress−strain curves of the dry and wet BP samples are displayed in Figure 4, and the mean values (n = 5, ±SD) of the Young modulus, tensile strength, and elongation at break are reported in Table 3.

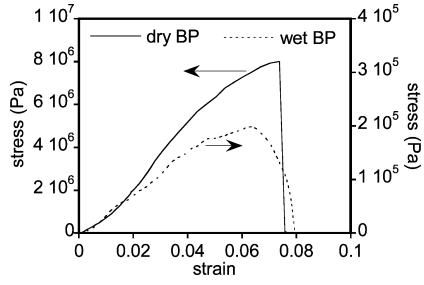

Figure 4. Tensile stress−strain curves of dry and wet BP.

The dry BP stress−strain curve showed a nearly elastic deformation of the sample before the breaking and a fragile fracture. After BP soaking in water, a drastic reduction in Young modulus and tensile strength occurred, while the elongation at break did not significantly change with respect to the dry sample. Moreover, the wet BP breaking showed a partial ductile

Table 3. Tensile Mechanical Properties of Dry and Wet BP[a]

sample	Young modulus (MPa)	tensile strength (MPa)	strain at break (%)
dry BP	160 ± 5	8 ± 1	7 ± 1
wet BP	4 ± 1	0.20 ± 0.01	5 ± 2

[a]Each value represents the mean value ± standard deviation of five independent experiments.

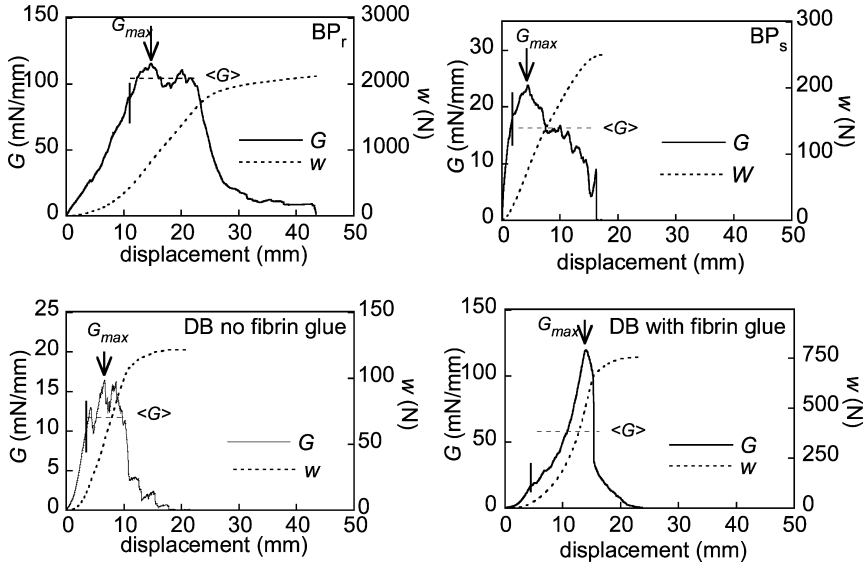

Figure 5. Peeling strength (G) and peeling work (w) as a function of sample displacement during the peeling test for BP$_r$, BP$_s$, bare DB, and DB fixed onto the biological substrate by fibrin glue.

fracture, as evidenced by the plastic deformation in the 0.04−0.07 strain region followed by a progressive reduction of the stress. The mechanical properties of buckypaper, as of other nonwoven fibrous materials, are determined by the interfiber interactions for small deformation and by fiber entanglements or bundling in the plastic strain region up to the break.

In general, it was observed that the mechanical properties of buckypaper are determined by the number density of interbundle junctions, which are much weaker than nanotubes themselves or interbundle interactions.[35] The number of contacts among the nanotubes or nanotube bundle depends, in turn, on buckypaper porosity and bundle diameter. Kastanis et al.[36] suggested that the higher is the MWCNT oxidation degree the higher is the colloidal stability of the suspension used to prepare the buckypaper and the density and homogeneity of the obtained film. Then, the samples prepared from highly oxidized CNT showed enhanced mechanical properties. Moreover, Spitalsky et al.[37] attributed the high Young modulus and strength at the break of buckypaper produced from nitric acid treated MWCNT to the interbundle hydrogen bond interactions. Whitten at al.[38] reported that a dry buckypaper sample (from single-walled CNT) in equilibrium with atmospheric water vapor contained a small amount of water and that attracting capillary forces of condensed water bridges occurring in the nanotube−nanotube contacts contributed to the mechanical stiffening of BP. In the water swollen state, the excess of liquid filling the pores weakened the nanotube junctions, as evidenced by a moderate decrease in the BP Young modulus, but it increased the strength at the break.

The water swelling of our highly oxidized BP affects the material mechanical properties. In fact, the experimental results showed that this polar liquid was able to drastically weaken the interbundle interactions due to the establishment of hydrogen bonds with the polar groups of oxidized CNT. The decrease in interaction strength reduced the sample modulus and facilitated the sliding of adjacent bundles, allowing the small plastic deformation observed in wet BP. The importance of polar interactions on BP mechanical properties is supported by the unchanging of mechanical behavior when swollen in *n*-dodecane. On the other hand, the elongation at break, probably depending on CNT or CNT bundle disentangling, was not affected by water.

Adhesion Test Results. The BP surface adhered promptly and firmly on the wet and soft biological tissue. In order to quantify the adhesion strength, both peeling at 90° and shear tests were carried out by measuring the force necessary to detach BP$_r$ and BP$_s$ surfaces from the biological tissue by moving the sample apart from the substrate in a direction perpendicular (peeling test at $\varphi = 90°$) or parallel (shear test) to the interface between the two materials. For rigid inextensible materials and without bending stiffness, the peeling strength G is defined as

$$G = \frac{F}{b} \times (1 - \cos \phi) \tag{5}$$

where F is the measured peeling force, b is the sample width, and φ is the peeling angle. Actually, eq 5 does not take into account the substrate deformation, resulting local angle variation, bending stiffness of the peeled material, and some geometrical factors such as the distance between the substrate fixed edges and the peeled sample. Therefore, the eq 5 underestimates the peeling strength as reported by Steven-Fontain et al..[39] A representative plots of G vs the displacement of BP$_r$, BP$_s$, bare Dulex Bard (DB) membrane, and DB sealed with fibrin glue are displayed in Figure 5. In the graphs, the peeling work w was also reported. w is defined as

$$w = \int_0^l G\mathrm{d}l \tag{6}$$

where l is the sample displacement. The maximum value (w_{max}) reached at the end of the experiment represents the whole work needed to completely detach the sample from the biological tissue. The results of the peeling tests are reported in Table 4.

Typically, after a transient zone where the deformation of the compliant biological substrate occurs, the separation between the two materials begins and propagates. The beginning of the interface fracture is indicated in Figure 5 by the vertical bar. The mean value of the peeling strength over the fracture zone (<G>) and the maximum (G_{max}) peeling strength were measured after the first transient zone. As for the BP$_r$ sample,

dx.doi.org/10.1021/am400543s | ACS Appl. Mater. Interfaces 2013, 5, 4340−4349

Table 4. Peeling and Shear Test Data[a]

sample	G_{max} (mN mm^{-1})	<G> (mN mm^{-1})	w_{max} (N)	τ_{max}(mN mm^{-2})
BP_r	140 ± 50	100 ± 20	2200 ± 100	20 ± 3[b]
BP_s	31 ± 7	15 ± 3	200 ± 50	5 ± 2
DB no fibrin glue	15 ± 6	11 ± 5	100 ± 30	0.3 ± 0.2
DB with fibrin glue	120 ± 50	60 ± 20	700 ± 200	5 ± 3

[a]Each value represents the mean value ± standard deviation of five independent experiments. [b]The sample breaks before the adhesion failure.

it can be observed that before the peeling process started the substrate underwent a large deformation, up to about 10 mm, because of the tight adhesion of BP_r to the compliant biological tissue. Then, the fracture propagated with a strength fluctuation around the average value <G> = 100 mN mm^{-1}. At the end of the test, the peeling strength decreased progressively because of the not uniform detachment of BP_r from the substrate.

Although the wicking tests did not allow the assessing of possible differences in porosity between the two BP sides, the peeling results gave a clear indication about the influence of surface morphology on BP adhesive behavior. The smooth BP_s surface, in fact, showed significant lower values of peeling strength and peeling work than those recorded for the porous and nubby BP_r side. As it will be discussed later, the BP_s surface flatness and compactness could explain the observed differences.

In surgical procedure, the DB fabric is usually fixed to the damaged tissue by perforating fixation devices (suture or tacks). In fact, the bare prosthesis shows poor adhesion toward biological tissues, as also shown by our experiments in which DB possessed adhesive properties 10 times lower than those observed for BP_r (Table 4). To avoid suture stitches and reduce post-operative complications, some studies reported the use of fibrin glue to improve DB adhesion to the biological substrate.[40,41] Therefore, in this study, the adhesion behavior of DB membrane either simply placed on the tissue or fixed to the tissue with fibrin glue was also investigated and compared to BP. As shown in Figure 5, the adhesion strength of DB with fibrin glue resulted to be largely inhomogeneous. In fact, an intense step rise of the peeling strength at about 15 mm displacement as well as a high dispersion of <G> values and a low w_{max} value were observed. Moreover, although the maximum G value was comparable with that recorded for BP_r, <G>was halved and the maximum work (w_{max}) reduced to one-third.

The shear tests were performed to assess the adhesion strength of the sample stressed by a lateral movement that better mimic the real stress applied to the prosthesis in the implantation site. In Figure 6, the shear adhesion strength τ, defined as the ratio between the recorded shear force and the initial interface area, is reported as a function of the sample displacement. In Table 4, the maximum shear strength (τ_{max}) is reported as the mean of five measurements (±SD).

The DB membrane adhered to the biological tissue with negligible strength, and fibrin glue was necessary to anchor this commercial fabric to the tissue. The adhesion of DB fixed with fibrin glue decreased after about 5 mm displacement and failed at about 8 mm. Although DB fixed with fibrin glue showed a good adhesion in the peeling tests (Table 4), in the shear experiments the sample easily detached from the substrate. In

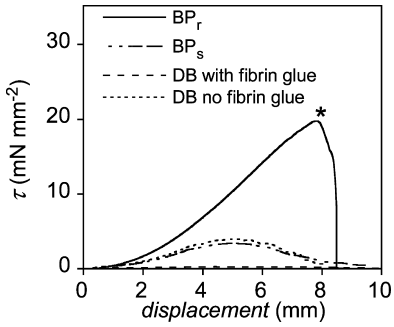

Figure 6. Shear adhesion strength of BP_r, BP_s, bare DB, and DB fixed with fibrin glue as a function of the sample displacement. (*) Sample breaks before the adhesion failure.

particular, a significantly better adhesion to the biological substrate was observed for BP_r than DB fixed with fibrin glue (Table 4). In fact, during the test on BP_r, a large deformation of the biological tissue occurred without interface fracture. At a greater displacement, the adhesion strength exceeded the load-bearing limit of the partially wet buckypaper foil, and sample break occurred before detachment started (indicated by * symbol in Figure 6). Then, the maximum shear adhesion strength reported for BP_r should be considered as the lowest limit of the actual τ_{max}. If the recorded shear force at break is normalized by the sample section, instead of the material interface area, a stress at break (tensile strength) of 2 MPa is obtained, which is intermediate between the values found for dry and wet BP (Table 3). This is due to the partial water or physiologic fluid absorption into the sample during the shear test. The smooth BP_s surface showed a significantly lower shear adhesion strength than the rough BP_r side (Table 4), revealing the strong influence of surface morphology on the shear adhesion.

All the adhesion experiments were carried out by using dry BP. By repeating a second peeling or shear test soon after the first sample detachment occurred, a decrease in the adhesion strength up to 80% was recorded. This behavior can be related to the drying of the tissue surface and/or to the liquid absorption into BP during the first experiment. In fact, the residual fluid into the material pores obstacles the further liquid suction driven by negative capillary pressure, causing an adhesion reduction. When BP is completely imbibed by water, the adhesion on the animal substrate was nearly null. Moreover, being negligible, the adhesion strength of BP on soft tissue dried after long exposure to ambient condition, and direct short-range interaction between the BP polar groups and the biological surface was excluded.

DISCUSSION

Because of the complexity of the studied system, it is difficult to model the high adhesiveness of buckypaper to the wet soft biological tissue. On the basis of previous investigations on the effect of surface roughness on adhesion and friction[42] and considering the strategies evolved by some animals to move and climb on rough or smooth surfaces, an interpretation of the obtained results is here following given.[1,3,43,44] First of all, it must be stressed that if a stable adhesion on wet soft biological tissues is requested, BP does not have to strictly match the broad criteria mandatory for animal locomotion that are reusability, reversibility, and substrate tolerance. In fact, in dynamic condition, a soft and wet pad can undergo a rapid

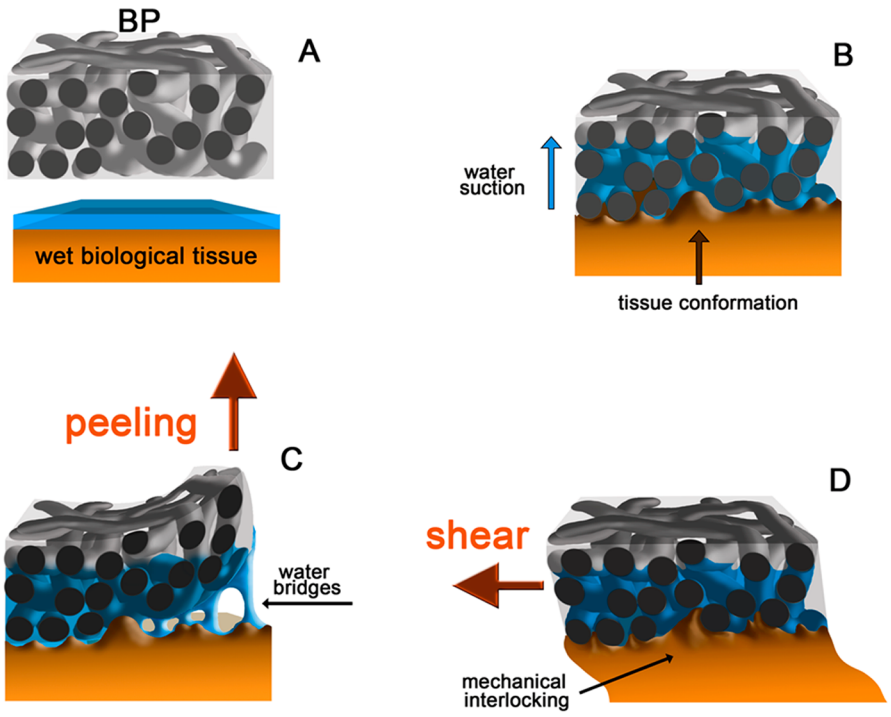

Figure 7. Scheme of the proposed buckypaper adhesion mechanism. (A) BP and the wet biological tissue before the contact. (B) Water suction and soft tissue conformation after its contact with BP. (C) Water bridge formation during BP detachment from the tissue in peeling tests. (D) BP−tissue interface mechanical interlocking hampering shear movement in shear tests.

deterioration, contamination, and liquid consumption. In addition, it does not permit rapid attachment and detachment cycles in presence of a viscous fluid. On the other hand, a porous and rigid surface could not adhere to an elastic substrate because of the low contact area and the high stored elastic energy associated with the bending of the surface. As for permanent adhesion, the problem could be reversed. Is it possible to design a material able to adhere to a smooth compliant surface in wet condition? What is the effect of the material stiffness, roughness, and porosity on the adhesion to the soft substrate? We believe that there are five BP key features contributing to the material adhesive behavior: (i) MWCNT hydrophilicity, (ii) nanosized open porosity, (iii) high porosity, (iv) surface nanoroughness, and (v) mechanical stability. All these specific properties combined in one material render BP unique.

Although carbon nanotubes are hydrophobic, physical or chemical oxidizing treatments can provide them with amphiphilic properties by introducing polar functional groups on nanotube edges or defects. XPS analysis showed that the BP used in this study had high oxygen content due to the presence of phenols, ethers, ester, and carboxylic acid. The hydrophilic component improved the BP wetting in water but did not provoke the disaggregation of nanotube bundles and network or a drastic drop in BP mechanical stability. The apparent BP water contact angle <90° and the nanodimension of the pores formed by the intertube space favored the rapid absorption of water that, differently from what happens in other types of nanofiber webs, did not cause sample swelling or collapse. In fact, although the liquid infiltration led to the weakening of intertube interactions, as shown by the reduction of BP tensile mechanical properties (Table 3), the high rigidity of carbon nanotubes prevented porosity or morphology modification. When the rough and porous BP_r side came in contact with the compliant wet surface, the water suction, driven by the negative capillary pressure, forced the compliant substrate to plastically yield and approach the BP surface (Figure 7A,B).

Neglecting any repulsive elastic force between the two surfaces, the lower limit of water layer thickness between the compliant biologic tissue and the hard buckypaper surface will be, in first approximation, of the same order of magnitude of the equivalent pore radius R (Table 2).[3] Interestingly, such a value is very close to that found between the tree frog toe or stick insect pad and glass substrates.[43,44] Capillary adhesion is, in fact, the strategy used by these animals for locomotion. Their noncompact and elastically soft pads adhere to surfaces by means of the injection of a wetting liquid into the contact area. It was observed that both the shear and normal adhesion increases when the fluid film thickness decreases. The adhesion mechanism in part also resembles that adopted by echinoderms that have soft viscoelastic foot discs able to move in close proximity to the substrate and replicate the rough substratum profile.[45]

Moreover, the high BP_r surface roughness ensures both a high contact area between BP and the conformable biologic tissue, well above the geometrical one (Table 1), and a high peeling fracture toughness due to a multiple arrest and initiation mechanism of the interface fracture.[46] During the BP pull-off, water moves back at the interface, and the adhesion is mediated by the liquid bridges forming between the buckypaper surface nano-asperities and the substrate (nano-capillary bridges network) (Figure 7 C).[7,42] By taking into account the contact-line splitting mechanism, an adhesion strength enhancement can be expected with the increase in the independent contact patches and in the overall length of the contact contour perimeter.[47] Such an effect is especially true on the rough and nubby BP_r surface. Although the wicking experiments gave just an averaged value of the pore size, not

dx.doi.org/10.1021/am400543s | ACS Appl. Mater. Interfaces 2013, 5, 4340−4349

taking into account the morphological asymmetry of the two BP sides, the adhesion tests clearly evidenced the influence of the roughness and porosity on adhesion mechanism. In fact, the smoother and more densely packed BP_s surface showed a significant lower adhesion strength, probably related to the lower water suction rate and BP−tissue interface area (Table 1). Differently from other patterned surfaces endowed with a nanopillar array, the high BP open porosity permits the rapidly drain of the excess of water or biological fluid on the tissue. By inserting in eq 4, the thickness of the BP foil, $d = 200 \times 10^{-6}$ m, a diffusion time of water in a perpendicular direction to the BP foil plane of about 1 s, could be inferred. As far as the interface stability in shear experiments is concerned, it is possible to hypothesize that besides the direct thin water layer mediating the interaction between the two nearby surfaces (tacky regime)[6] mechanical interlocking occurs between the large and deep asperities of the rigid BP_r surface and the soft biological tissue lobes, as schematically displayed in Figure 7 D. The proposed shear adhesion mechanism is supported by the results obtained on the BP_s side. In fact, the surface flatness and the shallow asperities (Figure 1 and Table 1) of this face offered a minor resistance to the interface slippage.

The shear adhesion strength obtained by putting in contact BP_r with the biological tissue (20 mN mm^{-2}) was higher than that found between an optimized micropillar-based silicone rubber adhesive and the pig small intestinal surface.[4] In addition, the BP_r shear adhesion strength was found to be comparable with that observed on a poly(glycerol sebacate acrylate) (PGSA)-optimized nanopatterned surface coated with oxidized dextran (DXTA).[5] However, in this latter system, the interface adhesion was enhanced by covalent cross-linking of DXTA aldehyde groups with the tissue.

In this study, a commercial prosthetic fabric, DB, was also tested. The hydrophobic DB showed poor adhesion on the biological substrate. When sealed to the biological tissue by fibrin glue, DB fabric showed good peeling adhesion strength, comparable with that of BP. Probably, the initially fluid sealant penetrated into the fabric macropores and, after cross-linking by thrombin, the formed fibrin gel adhered to the prosthesis by interlocking mechanism. On the other hand, the compliance of the visco-elastic gel and the softness of the fabric hampered a tight adhesion to the biological substrate with a consequent failure in the shear adhesion.

The adhesion properties of BP in wet condition could be exploited for the preparation of self-gripping tapes to be used in biomedical application, favoring the reduction in the use of conventional prosthesis fixation methods, often causing post-operative complications.

However, the assessment of toxicity and biocompatibility of BP represents a fundamental issue in the light of the possible applications of the material in the biomedical field. Although, as reported in the Introduction, different BP-based medical devices have been proposed, but few are the researches about their biocompatibility in mammalians. In previous in vivo studies on rats carried out by our group, it has been observed that BP induced a moderate inflammatory reaction.[19] Two weeks after BP implantation, a cicatrization reaction with a scar organization and fibrosis have been recorded. Further in vivo studies on rats and rabbits are currently in progress to evaluate not only the effect of BP on tissue local responses and neuro-vegetative animal behavior but also BP adhesion onto the surrounding tissues. Preliminary results evidenced that the BP elicited minimal adverse tissue response, comparable to that observed for commercial prosthetic mesh (including DB). In addition, BP showed rapid, strong, and stable integration with the surrounding tissues. Finally, an increased adhesion strength to the biological substrate was observed after 35 days from the implantation.

Today, there are conflicting data concerning the safety and biocompatibility of carbon nanotubes.[48] However, oxidized CNT are reported to be more toxic than the pristine ones because of their higher dispersion in water.[49] Then, great care should be taken to evaluate the possible release of the nanotubes or nanotube aggregates from implanted BP.

CONCLUSION

Peeling and shear adhesion tests showed that the rough surface of buckypaper obtained from oxidized MWCNT was able to strongly and promptly adhere to soft and wet animal internal tissues. BP hydrophilicity and nanoporosity favored the rapid suction of water or biological fluid thus promoting the adhesion of the biological tissue. At the same time, the MWCNT mechanical rigidity ensured the stability of the porous structure. Although BP biocompatibility and long-term safety should be definitively assessed, the BP high adhesiveness could be exploited in the medical field for the preparation of bioadhesive tapes for abdominal prosthetic surgery or wound closure.

ASSOCIATED CONTENT

Supporting Information

Scheme of the instrumental setup used for peeling and shear tests. This material is available free of charge via the Internet at http://pubs.acs.org.

AUTHOR INFORMATION

Corresponding Author

*E-mail: andrea.martinelli@uniroma1.it.

Author Contributions

The manuscript was written through contributions of all authors. All authors have given approval to the final version of the manuscript.

Notes

The authors declare no competing financial interest.

ACKNOWLEDGMENTS

We thank Agostino Eusepi for his precious help in animal housing and MIUR (Ricerche Universitarie) for financial support.

REFERENCES

(1) Peattie, A. M. *J. Comp. Physiol., B* **2009**, *179*, 231−239.
(2) Kwak, M. K.; Pang, C.; Jeong, H.-E.; Kim, H.-N.; Yoon, H.; Jung, H.-S.; Suh, K.-Y. *Adv. Funct. Mater.* **2011**, *21*, 3606−3616.
(3) Persson, B. N. J. *J. Adhes. Sci. Technol.* **2007**, *21*, 1145−1173.
(4) Kwon, J.; Cheung, E.; Park, S.; Sitti, M. *Biomed. Mater.* **2006**, *1*, 216−220.
(5) Mahdavi, A.; Ferreira, L.; Sundback, C.; Nichol, J. W.; Chan, E. P.; Carter, D. J. D.; Bettinger, A. C. J.; Patanavanich, S.; Chignozha, L.; Ben-Joseph, E.; Galakatos, A.; Pryor, H.; Pomerantseva, I.; Masiakos, P. T.; Faquin, W.; Zumbuehl, A.; Hong, S.; Borenstein, J.; Vacanti, J.; Langer, R.; Karp, J. M. *Proc. Natl. Acad. Sci. U.S.A.* **2005**, *105*, 2307−2312.
(6) Persson, B. N. J. *J. Phys.: Condens. Matter* **2008**, *20*, 315007−315018.
(7) Samoilov, V. N.; Sivebaek, I. M.; Persson, B. N. J. *J. Chem. Phys.* **2004**, *121*, 9639−9647.

(8) Liu, L.; Ma, W.; Zhang, Z. *Small* **2011**, *7*, 1504−1520.
(9) Yang, W.; Thordarson, P.; Gooding, J. J.; Ringer, S. P.; Braet, F. *Nanotechnology* **2007**, *18*, 412001−412013.
(10) Loftus, D. J. Provision of Carbon Nanotube Bucky Paper Cages for Immune Shielding of Cells, Tissues, and Medical Devices. U.S. Patent 7,070,923, June 4, 2006.
(11) Loftus, D. J.; Leng, T.; Fishman, P. H. Bucky Paper as a Support Membrane in Retinal Cell Transplantation. U.S. Patent 7,135,172, November 14, 2006.
(12) Simmons, T. J.; Lee, S.-H.; Park, T.-J.; Hashim, D. P.; Ajayan, P. M.; Linhardt, R. J. *Carbon* **2009**, *47*, 1561−1564.
(13) Weber, J.; Holman, T. J.; Eidenschink, T.; Chen, J. J. Using Bucky Paper As a Therapeutic Aid in Medical Applications. U.S. Patent 8,354,120, January 15, 2013.
(14) Weber J., Holman T. J. Medical Devices and Methods of Making the Same. U.S. Patent Application 0260355, November 24, 2005.
(15) Correa-Duarter, M. A.; Wagner, N.; Rojas-Chapana, J.; Morsczeck, C.; Thie, M.; Giersig, M. *Nano Lett.* **2004**, *4*, 2233−2236.
(16) Gheith, M. K.; Pappas, T. C.; Liopo, A. V.; Sinani, V. A.; Sup Shim, B.; Motamedi, M.; Wicksted, J. P.; Kotov, N. A. *Adv. Mater.* **2006**, *18*, 2975−2979.
(17) Whitten, P. G.; Gestos, A. A.; Spinks, G. M.; Gilmore, K. J.; Wallace, G. G. *J. Biomed. Mater. Res., Part B* **2007**, *82*, 37−43.
(18) Wallace, G. G.; Moulton, S. E.; Whitten, P. G.; Lyman, C. M. Biocompatible composites. U.S. Patent Application 0023101, January 28, 2010.
(19) Bellucci, S.; Chiaretti, M.; Cucina, A.; Carru, G. A.; Chiaretti, A. I. *Nanomedicine* **2009**, *4*, 531−540.
(20) Scofield, J. H. *J. Electron Spectrosc. Relat. Phenom.* **1976**, *8*, 129−137.
(21) Dang-Vu, T.; Hupka, J. *Physicochem. Probl. Miner. Process.* **2005**, *39*, 47−65.
(22) Daniel, S.; Rao, T. P.; Rao, K. S.; Rani, S. U; Naidu, G. R. K.; Lee, H.-Y.; Kawai, K. *Sens. Actuators, B* **2007**, *122*, 672−682.
(23) Jang, X.; Bin, Y.; Matsuo, M. *Polymer* **2005**, *46*, 7418−7424.
(24) Barber, A. H.; Cohen, S. R.; Wagner, H. D. *Phys. Rev. B* **2005**, *71*, 115443−115447.
(25) Mattia, D.; Rossi, M. P.; Kim, B. M.; Korneva, G.; Bau, H. H.; Gogotsi, Y. *J. Phys. Chem. B* **2006**, *110*, 9850−9855.
(26) Volkov, A. N.; Zhigile, L. V. *ACS Nano* **2010**, *4*, 6187−6195.
(27) Kvande, I.; Zhu, J.; Zhao, T.-J.; Hammer, N.; Rønning, M.; Raaen, S.; Walmsley, J. C.; Chen, D. *J. Phys. Chem. C* **2010**, *114*, 1752−1762.
(28) Ago, H.; Kugler, T.; Cacialli, F.; Salaneck, W. R.; Shaffer, M. S. P.; Windle, A. H.; Friend, R. H. *J. Phys. Chem. B* **1999**, *103*, 8116−8121.
(29) Kundu, S.; Wang, Y.; Xia, W.; Muhler, M. *J. Phys. Chem. C* **2008**, *112*, 16869−16878.
(30) Blanchard, N. P.; Hatton, R. A.; Silva, S. R. P. *Chem. Phys. Lett.* **2007**, *434*, 92−95.
(31) Xia, W.; Wang, Y.; Bergsträßer, R.; Kundu, S.; Muhler, M. *Appl. Surf. Sci.* **2007**, *254*, 247−250.
(32) Speranza, G.; Minati, L. *Diamond Relat. Mater.* **2007**, *16*, 1321−1324.
(33) Coleman, J. N.; Khan, U.; Blau, B. J.; Gunko, Y: K. *Carbon* **2006**, *44*, 1624−1652.
(34) Callegari, G.; Tyomkin, I.; Kornev, K. G.; Neimark, A. V.; Hsieh, Y.-L. *J. Colloid Interface Sci.* **2011**, *353*, 290−293.
(35) Blighe, F. M.; Lyons, P. E.; De, S.; Blau, W. J.; Coleman, J. N. *Carbon* **2008**, *46*, 41−47.
(36) Kastanis, D.; Tasis, D.; Papagelis, K.; Parthenios, J.; Tsakiroglou, C.; Galiotis, C. *Adv. Compos. Lett.* **2007**, *16*, 243−248.
(37) Spitalsky, Z.; Aggelopoulos, C.; Tsoukleri, G.; Tsakiroglou, C.; Parthenios, J.; Georga, S.; Krontiras, C.; Tasis, D.; Papagelis, K.; Galiotis, C. *Mater. Sci. Eng., B* **2009**, *165*, 135−138.
(38) Whitten, P. G.; Spinks, G. M.; Wallace, G. G. *Carbon* **2005**, *43*, 1891−1896.
(39) Steven-Fountain, A. J.; Atkinsa, A. G.; Jeronimidisa, G.; Vincent, J. F. V.; Farrarc, D. F.; Chivers, R. A. *Int. J. Adhes.* **2002**, *22*, 423−430.
(40) Petter-Puchner, A. H.; Walder, N.; Redl, H.; Schwab, R.; Öhlinger, W.; Gruber-Blum, S.; Fortenly, R. H. *J. Surg. Res.* **2008**, *150*, 190−195.
(41) Topart, P.; Vandenbroucke, F.; Lozach, P. *Surg. Endosc.* **2005**, *19*, 724−727.
(42) Persson, B. N. J.; Albohr, O.; Tartaglino, U.; Volokitin, A. I.; Tosatti, E. *J. Phys.: Condens. Matter* **2005**, *17*, R1−R62.
(43) Federle, W.; Barnes, W. J. P.; Baumgartner, W.; Drechsler, P.; Smith, J. M. *J. R. Soc. Interface* **2006**, *3*, 689−697.
(44) Drechsler, P.; Federle, W. *J. Comp. Physiol., A* **2006**, *192*, 1213−1222.
(45) Santos, R.; Gorb, S.; Jamar, V.; Flammang, P. *J. Exp. Biol.* **2005**, *208*, 2555−2567.
(46) Ghatak, A.; Mahadevan, L.; Chung, J. Y.; Chaudhury, M. K.; Shenoy, V. *Proc. R. Soc. London, Ser. A* **2004**, *460*, 2725−2735.
(47) Qian, J.; Gao, H. *Acta Biomater.* **2006**, *2*, 51−58.
(48) Firme, C. P.; Bandaru, P. R. *Nanomedicine: Nanotechnol., Biol., Med.* **2010**, *6*, 245−256.
(49) Bottini, M.; Bruckner, S.; Nika, K.; Bottini, N.; Bellucci, S.; Magrini, A.; Bergamaschi, A.; Mustelin, T. *Toxicol. Lett.* **2006**, *160*, 121−126.